



# Numerical modeling of the freefall of two-dimensional wedge bodies into water surface

Mohammad Izadi<sup>1</sup> · Parviz Ghadimi<sup>1</sup>  · Manouchehr Fadavi<sup>1</sup> · Sasan Tavakoli<sup>1</sup>

Received: 6 July 2017 / Accepted: 8 December 2017 / Published online: 15 January 2018  
© The Brazilian Society of Mechanical Sciences and Engineering 2018

## Abstract

In the current paper, two-dimensional freefall of wedge water entry is investigated in 1 degree of freedom. The defined problem is numerically studied using the STAR CCM+ software and by adopting an overset mesh approach. Three different chine wedges of 10°, 20°, and 30° deadrise angles are modeled. Kinematics of the considered wedges, impact loads, pressure, and the free-surface elevation around the considered wedges are presented. Based on the comparison of the computed vertical acceleration of the wedge of 20° deadrise angle against experimental data, it is determined that the proposed numerical method has relatively good accuracy in predicting the wedge response. The effects of deadrise angle and drop height on the kinematics of the wedges are also explored in different numerical simulations. Larger deadrise angle is found to yield lower and more transient vertical acceleration. It is demonstrated that impact force increases with an increase in depth, but finally approaches a constant value. Time histories of the pressure at three different points, located on the wedge wall, are also computed, indicating that an increase in the height leads to larger pressure at these points. However, when the mass is increased, the difference between the peak pressures at these points is strikingly reduced. Plots of the pressure distributions are also presented, which suggest that, as the submergence of the wedge increases, the pressure coefficient decreases. Furthermore, the pressure distributions indicate that, for the lighter wedge, the reduction in pressure coefficient is larger. Ultimately, the free surface elevation around a wedge during the freefall is presented. An increase in the pile-up is observed when the submergence height is increased, but for the wedge of 30° deadrise angle, the difference between free-surface profiles at specific times is far less than that of wedges of 10° and 20° deadrise angles.

**Keywords** 2D wedge · Water entry · Freefall · Hydrodynamic response · Computational fluid dynamics

## 1 Introduction

Water entry of solid bodies has always been considered an interesting and crucial problem for the naval architects and structural engineers. Accurate prediction of the forces acting on the sections entering water helps engineers design a better and safer structure, especially in the rough waters [1]. Furthermore, a good estimation of hydrodynamic pressure in such a phenomenon is an important key for accurately predicting the performance of high-speed

crafts in steady [2], unsteady [3–5], and even maneuvering motions [6]. On the other hand, most of the researchers in this field have frequently considered the water entry with constant vertical speed, but when a section enters the water, its speed varies overtime. In recent years, some new research has been carried out, aiming to determine the flow characteristics and impact loads during the freefall of the wedge. The current research also aims at providing wider results and understandings about this phenomenon through numerical approach. To this end, pressure field and response of the wedge falling into water are determined by solving Navier–Stokes equation with finite-volume method and by taking advantage of the volume of fluid scheme for capturing the free surface.

The physics of the water entry problem have been studied by a wide range of researchers. The starting point can be traced back to some classical works focusing on the landing of seaplanes. Von Karman [7] was a pioneer in this

---

Technical Editor: Jader Barbosa Jr..

✉ Parviz Ghadimi  
pghadimi@aut.ac.ir

<sup>1</sup> Department of Marine Technology, Amirkabir University of Technology, Hafez Ave, No 424, P.O. Box 15875-4413, Tehran, Iran

field. He presented a solution to the water entry problem using the momentum variation. Afterward, Wagner [8] re-studied this problem and indicated that a pile-up factor should be used in determining the free-surface position, which can provide a better prediction of the impact load. These classical methods were based on the potential theory in which viscosity and surface tension of the fluid were neglected, and the potential flow around the solid body was determined. Moreover, in both these classical methods, boundary conditions were assumed to be linear to simplify the simulation process. Finally, Wagner method was considered based on the flat disk approximation, but no result was provided for a wedge-shaped body. Considering some physical aspects of this phenomenon, many researchers have attempted to modify the previous Wagner solution [8]. These efforts ranged from consideration of the non-linear aspects of the problem [9–11] to derivation of the water entry solution for three-dimensional conditions [12, 13]. Moreover, some new modifications were also applied to model the asymmetric water entry [14, 15]. In addition to the analytical solutions developed by modification of the Wagner method [8], some other solutions have been introduced which considered the linear free-surface boundary conditions and used Schwartz–Christoffel conformal mapping technique [16–19]. However, all of these analytical methods, from Wagner method to Schwartz–Christoffel conformal mapping, were restricted to only potential flow, and were not able to determine the real flow around the rigid body, penetrating the water surface. As surface integrating methods gained popularity among researchers, the focus of some research was shifted from the classical Wagner methods toward the semi-analytical approach in which boundary conditions were assumed to be linear and were applied for modeling the splashed-up water line. In this context, Zhao et al. [20] carried out an initial study and used the splashed up and determined the free surface elevation utilizing the vertical velocity components on the free surface. Some other theoretical solutions were also performed by Vorus [21], Xu et al. [22], and Judge et al. [23]. The two latter research took the asymmetric condition and oblique speed into account, respectively. These methods involved the simulation of irrotational flow and the obtained solution could not expectedly offer any better result than analytical or numerical solution of the Navier–Stokes equations. This is while, in the real sea condition and especially when other ship motions are involved, the viscous tensions may play a vital role on the impact load, and even the breaking of the water jet needs to be simulated with more accuracy.

To obtain more accurate solutions and overcome the stated difficulty, some researchers have taken advantage of the computational fluid dynamics (CFD) methods and conducted different simulations. Explicit finite-element

method (FEM) was used by Stenius et al. [24, 25] to model the water entry of ship sections and predicted their hydroelastic behavior of the flexible wedges. Later, Wang et al. [26] presented a specific FEM-based approach for determining the impact loads acting on a wedge section penetrating the water with constant speed. They further developed their work for considering other conditions [27–29]. Smoothed particle hydrodynamics (SPH) is an alternative method which has also been used for analyzing this problem. Based on the observations of different researchers, this method is shown to provide good assessment for the water surface elevation, while the impact load is under-estimated. Using SPH method, Farsi and Ghadimi [30] conducted different simulations for water entry of wedge sections with constant speed, and later presented their results for twin-wedge sections with deck [31], asymmetric impact [32], and three-dimensional geometries [33]. In addition to these methods, finite-volume method (FVM) has also drawn the attention of many of researchers, mainly due to its proper accuracy, as claimed by Brizzolara et al. [34]. Using FVM, Fairlie-Clark and Tvitness [35] also computed forces acting on the wedge sections and determined the added mass force contribution in impact force. Adopting a different approach and utilizing the InterFoam solver in the OpenFoam software which uses the FVM and volume of fluid (VOF) techniques, Maki et al. [36] predicted the water surface elevation and hydrodynamic pressure acting on the body with reasonable accuracy. In a different study, Ghadimi et al. [37] simulated water entry of a circular cylinder with constant speed and later extended their simulations to the water impact of arbitrary bow sections [38, 39]. Shademani and Ghadimi [40–42] established an FEM-based FVM approach in which they simulated 2D and 3D water entry problems. More details about numerical methods and their accuracy in simulation of water entry problem can be found in the work of Brizzolara et al. [34]. Based on the surveyed literature, it is clear that these numerical studies were only performed to model the constant speed water entry problem. It is quite apparent that, while these schemes demonstrate (especially the FVM) great potential in solving flow around a wedge entering the water, they were not used to solve the free fall of a wedge and its dynamic response. However, during the operation of a ship, it is impossible that a ship exhibits a constant-speed water entry motion.

To provide more applicable results, some researchers have tried to solve the water entry of rigid bodies in freefall condition. Faltinsen et al. [43] performed an early research regarding this problem, where they used the added mass variation of a cylinder. On the other hand, Xu et al. [44, 45] made some efforts to analyze such a problem for the wedge sections using the surface integration in which non-viscous

fluid was studied. Recently, a new series of experimental works [46–49] has been conducted with this view of the water entry problem, all of which have utilized particle image velocimetry (PIV). In addition, Facci et al. [50, 51] have numerically solved 2D and 3D water entry problems applying InterDymFoam Solver in OpenFoam freeware and compared their results with experimental data before the chine wetting. Their 2D results were confined to a 25° deadrise wedge.

In the current paper, it is aimed to provide a numerical simulation pattern based on FVM approach for the freefall of 2D wedges with chine. There are some particularly useful features for the proposed method. First, it aimed to consider freefall motion, and as a result, the dynamic response of a wedge is determined. Furthermore, the chine wetting is also taken into consideration, and the targeted simulations are conducted for the time subsequent to chine wetting. Furthermore, the flow is assumed to be viscous, and consequently, the normal stresses are computed and the effect of viscosity on the response can also be ascertained. Moreover, unlike some of the previously reported simulations [50, 51], in which only the wedge body penetrates the water and moves downward, an overset region is adopted around the wedge, which moves with the wedge and experiences all of its motions. On the other hand, this work deals with a wider range of wedges. The defined problem is solved and the response including the acceleration, speed, and displacements is determined in each time step. In addition to these, pressure, impact force, and the water surface elevation are computed. The predicted results are compared against experimental and previous numerical results to evaluate the accuracy of the problem. Ultimately, the main targeted results including kinematics of wedge, impact load, pressure time history, pressure distribution, and free-surface elevation are computed. All the targeted results are presented for different wedges of 10°, 20°, and 30° deadrise angles.

## 2 Description of problem

Schematic of the problem considered in the current study is displayed in Fig. 1. As evident in this figure, a wedge with chine of mass  $M$  is located at the initial height of  $h_0$ , above the calm water line. The wedge is symmetric and has a width of  $B$  and deadrise angle of  $\beta$ . It is assumed that the wedge can freely fall into the water, while its angular and horizontal motions are confined. A right-handed coordinate system, denoted by  $Oxy$ , is considered on the calm water line, just under the wedge apex, by which the wedge position is identified. The initial speed of the wedge is assumed to be zero.

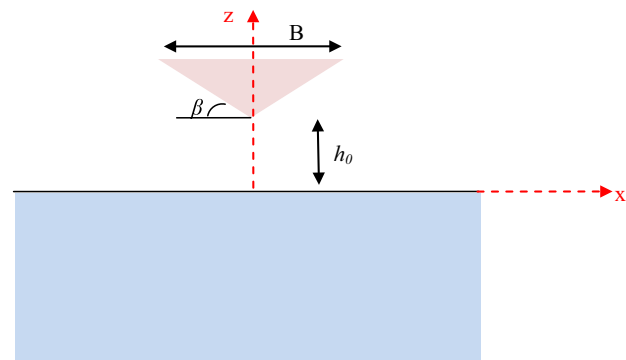


Fig. 1 Schematic of the considered problem

Using the defined coordinate system, equation of motion in vertical direction can be written as

$$M\ddot{z} = F_z - Mg \quad (1)$$

where  $\ddot{z}$  is the vertical acceleration and  $F_z$  is the total vertical force acting on the wedge. Parameter  $g$  represents the gravity acceleration and the term  $F_z$  is neglected before the water touches the wedge section. When the water touches the wedge section, the body gets wet and the water is piled-up, producing hydrodynamic pressure over the wedge, denoted by  $p$ . If the pressure and normal stresses,  $\sigma$ , are determined over all the wetted area, the impact force can be computed by

$$F_z = \int_S (pn_z + \sigma n_z) dl. \quad (2)$$

In this equation,  $n_z$  is the vertical component of the normal vector. In addition,  $S$  is the wetted area starts from the highest wetted point at the port and ends at the highest wetted point at the starboard. Since the wedge is considered to be symmetric and is constrained in other directions, these two points have similar heights at both sides of the wedge. This yields zero horizontal force and angular moment. In general, the force cannot be determined unless the water surface elevation and hydrodynamic pressure are determined. With this in mind, a numerical model is proposed in the current paper which is described in the next section.

## 3 Numerical method

### 3.1 Governing equations

The fluid domain consists of the air and water which are separated from each other by the free surface. The Mach number of the considered problem is far smaller than 0.3 in both the air and water, allowing us to use incompressible

fluid equations for analyzing the flow. Velocity vector  $\mathbf{u}$  at each point is given by

$$\mathbf{u} = u_x \mathbf{i} + u_y \mathbf{j}, \tag{3}$$

and the mass continuity equation is written as

$$\nabla \cdot \mathbf{u} = 0. \tag{4}$$

In addition, the momentum equation is

$$\frac{D(\rho \mathbf{u})}{Dt} = -\nabla p + \nabla \cdot \mu \mathbf{u} + \rho \mathbf{g} \tag{5}$$

where  $\rho$  is the density and  $\mu$  is the viscosity. The density is found by

$$\rho = \alpha \rho_w + (1 - \alpha) \rho_a \tag{6}$$

and viscosity is determined by

$$\mu = \alpha \mu_w + (1 - \alpha) \mu_a. \tag{7}$$

In Eqs. (6) and (7), subscripts  $w$  and  $a$  refer to the water and the air, respectively. Moreover,  $\alpha$  is the volume fraction of water in each cell which is governed by the equation:

$$\frac{\partial \alpha}{\partial t} + \nabla \cdot (\alpha \mathbf{u}) = 0. \tag{8}$$

To solve Eqs. (3) through (8), a numerical model is adopted within the STAR CCM+ software which has been utilized. Using FVM and semi-implicit method for the pressure-linked equations (SIMPLE) approach, the momentum and continuity equations are solved. In addition, the governing equation for  $\alpha$  is solved using High Resolution Interface Capturing (HRIC) scheme. Details of the problem setup are presented in the next sub-section.

### 3.2 Problem setup

The computational domain of the problem is illustrated in Fig. 2. The wedge apex is embedded on the vertical symmetry line of the domain. Two side walls are considered on

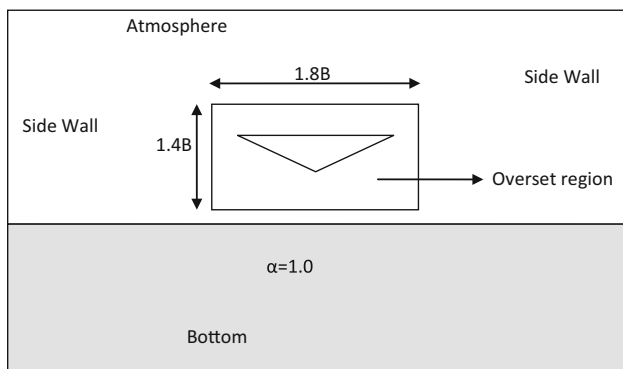


Fig. 2 Problem domain

the right and left sides of the wedge. On the solid walls, a free-slip condition is applied and gradient of volume fraction is considered to be zero. Bottom of the domain is considered to be a wall and its boundary condition is also assumed to be a free-slip condition, implying that pressure and velocity gradients are zero. In addition, the volume fraction gradient is set to be zero on the bottom wall. The upper side of the considered domain is considered to be an open patch from which the fluid can either enter or exit. On this patch, a relative pressure condition is applied. Moreover, the velocity gradient is set to be zero on this patch. Similar to other boundaries, the gradient of volume fraction is also assumed to be zero on this boundary. The wedge is initially placed at the vertical position of  $h_0$  above the calm water. The boundary condition for the wedge surface is taken to be no-slip boundary. On this boundary, pressure gradient along the direction perpendicular to the wall is zero. Below the water line,  $\alpha$  is set to be 1.0 which implies that there is water beneath this line. Details of the boundary conditions are presented in Table 1. The length of the considered domain is assumed to be  $12B$  and its depth is taken to be  $10B$ .

To analyze the problem, the initial vertical speed is assumed to be zero. Furthermore, the water line is set to be at rest, as an initial condition. A mass  $M$  is assumed for the wedge which causes a weight force, leading to the freefall of the wedge downward.

### 3.3 Mesh setup

To numerically investigate the problem, an overset mesh grid is generated. This type of meshing approach increases the accuracy of the solution near the far-field boundaries. In addition, small mesh is only produced near the moving body and free surface. As a result of this approach, the computation process is reduced. A schematic of the overset mesh for the current problem is displayed in Fig. 3, which consists of an overall and a close-up view of the mesh. As evident in the overall view of the mesh, an overset region surrounding the 2D wedge is considered. This region is set to be  $1.8B \times 1.4B$  in size. In addition, it is observed in the closed up view that around the wedge apex, where the possible water spray passes, the volumes appear to be

Table 1 Defined boundary conditions prescribed on the boundaries

Boundary	Velocity	Pressure	Volume fraction
2D wedge	$\mathbf{u} = \dot{x} \mathbf{i} + \dot{y} \mathbf{j}$	$\frac{\partial p}{\partial \mathbf{n}} = 0$	$\frac{\partial \alpha}{\partial \mathbf{n}} = 0$
Atmosphere	$\frac{\partial \mathbf{u}}{\partial \mathbf{n}} = 0$	$p = 0$	$\frac{\partial \alpha}{\partial \mathbf{n}} = 0$
Bottom and side walls	$\frac{\partial \mathbf{u}}{\partial \mathbf{n}} = 0$	$\frac{\partial p}{\partial \mathbf{n}} = 0$	$\frac{\partial \alpha}{\partial \mathbf{n}} = 0$

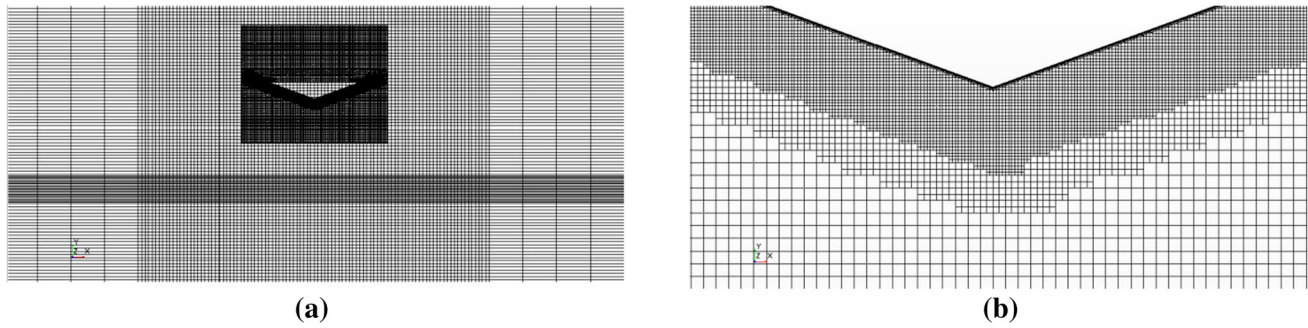


Fig. 3 a Overall view of the mesh and b close up view around the wedge

small. Finally, the mesh around the calm water surface is set to be fine. To offer more information regarding the mesh, the movements of the wedge with an overset region around it are shown at three different times, as shown in Fig. 4.

## 4 Validation

### 4.1 Mesh study

To find the most optimum mesh that is appropriate for the current freefall problem, the response of a wedge of 20° deadrise angle is examined. The wedge height is assumed to be 0.61 m and its mass is 124 kg. Six different mesh sizes are considered. Details of these meshes are shown in Table 2. Accordingly, the vertical acceleration, normal force, and vertical velocity of the 2D wedge is simulated by each of these mesh sizes and the results are compared against each other. The comparison is illustrated in Fig. 5. As evident in this figure, results of case 1 are undesirable in computing all three parameters. For example, large fluctuations are observed in the computed acceleration and vertical force when case 1 is used. On the other hand, it is observed that results of cases 2 and 3 indicate smaller force, smaller vertical acceleration, and smaller vertical velocity. It can also be seen that using cases 4, 5, and 6,

Table 2 Considered mesh sizes for the mesh study

Case	Number of cells
Case 1	7756
Case 2	11,467
Case 3	26,052
Case 4	90,762
Case 5	179,242
Case 6	500,246

similar values are determined for vertical force, acceleration, and vertical velocity of the wedge. By considering these details, mesh size 4 is adopted for solving the current problem. The results of this mesh are similar to those of mesh 5 and mesh 6, but the number of mesh elements in this case is smaller than the other cases.

### 4.2 Comparison with the previous results: pressure

For validation of the predicted pressure, the water entry of constant velocity is modeled for different wedges which have previously been considered in the famous numerical study conducted by Zhao and Faltinsen [20]. The computed pressures are compared against the numerical results [20], as shown in Fig. 6. As observed in this figure, the pressure distribution is in good agreement with the numerical

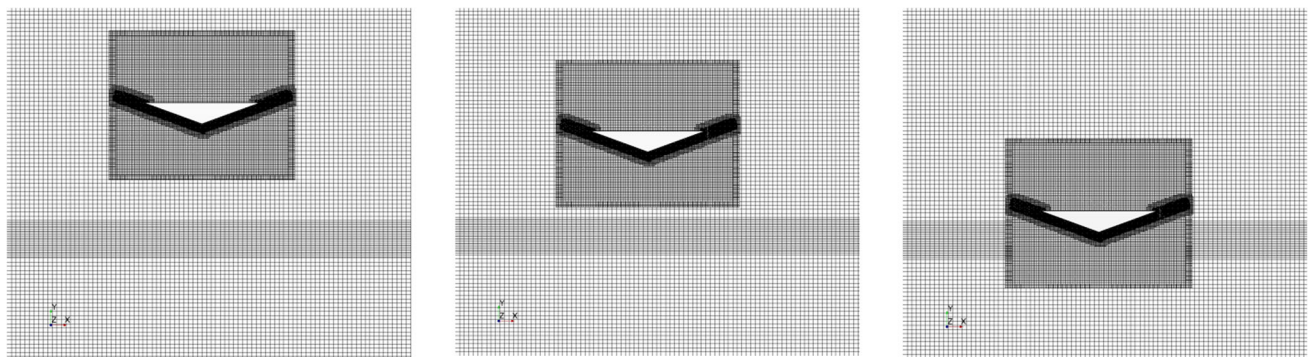
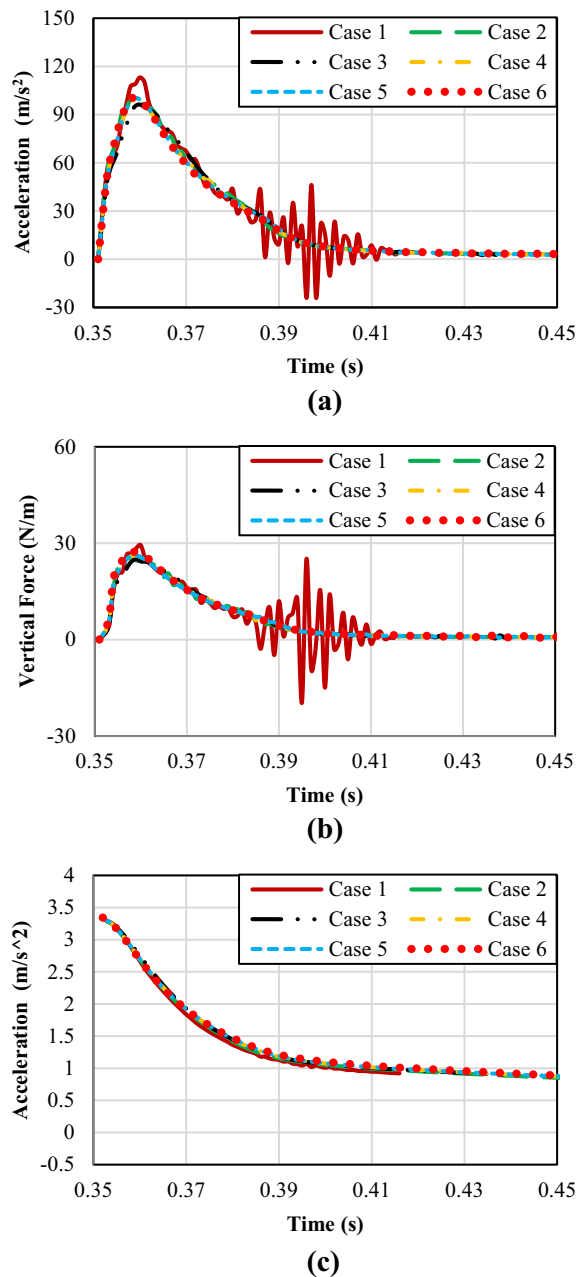


Fig. 4 Falling of the wedge and the overset region moving with it, at three different times



**Fig. 5** Grid study of the free fall of W2 model with mass of 124 kg and initial height of 0.61 m: **a** vertical acceleration, **b** vertical force, and **c** vertical velocity

results. The largest error between these methods in predicting the pressure corresponds to the wedge of 10° deadrise angle and this can be attributed to the peak of pressure. In other cases, the trends are in good agreement, and the peak pressures are relatively similar. Therefore, one may conclude that the present method provides reasonable accuracy in predicting the pressure distribution.

### 4.3 Comparison with the previous result of Xu et al. [22]

After verifying the accuracy of the presented numerical simulation in predicting the pressure, its accuracy in computing the kinematics of the wedges in freefall is assessed. For this purpose, three different wedges are considered, which are illustrated in Table 3. Based on the information provided in this table, these wedges have three different deadrise angles of 10°, 20°, and 30°. Two different masses and drop heights are also considered for the W2 model, while other examined wedges are numerically modeled for one mass and one drop height. The defined W2 model was previously studied by Xu et al. [22] which is hereby used for verifying the accuracy of the proposed method.

Kinematics of the wedge including acceleration, entry depth, and vertical velocities are also computed. The entry depth and vertical velocity are not presented in this section, but they will be reported later in the result section. A comparison of the predicted vertical acceleration against experimental data for the lighter cases of W2 model is displayed in Fig. 7, which contains three different drop heights of 0.61, 1.22, and 1.83 m. As observed in this figure, there is good agreement between the experimental data and the results of the current simulations. The trend of vertical acceleration as a function of time is similar to that of experimental data in all cases. The results of the numerical models show that the wedge touches the water, reaches its maximum acceleration, and approaches a final constant value, approximately at the recorded time of the experiments. The peaks of the vertical acceleration for all three drop heights are in good agreement with the experimental data. In the case of the lowest drop height, the maximum values are very close to each other, and the corresponding error is below 7%. For the other two cases, error is slightly larger which is related to the initial drop height. The error associated with the prediction of the maximum vertical acceleration of the case with the largest drop height is 18.2%. Larger initial drop height means larger impact speed at the time the wedge reaches the water, which leads to larger errors at that time. It is evident that the errors highly decrease after this time. That is, the larger drop height adversely affects the accuracy at the onset of the impact, and subsequently, errors reduce.

Comparison of the predicted vertical accelerations against experimental data for the W2 model with larger mass of 249 kg is demonstrated in Fig. 8. Similar to the lighter case, three different initial drop heights are simulated. For this case, as indicated for the lighter case, the best accuracy can be seen for the smallest drop height. In addition, the errors associated with the drop height of

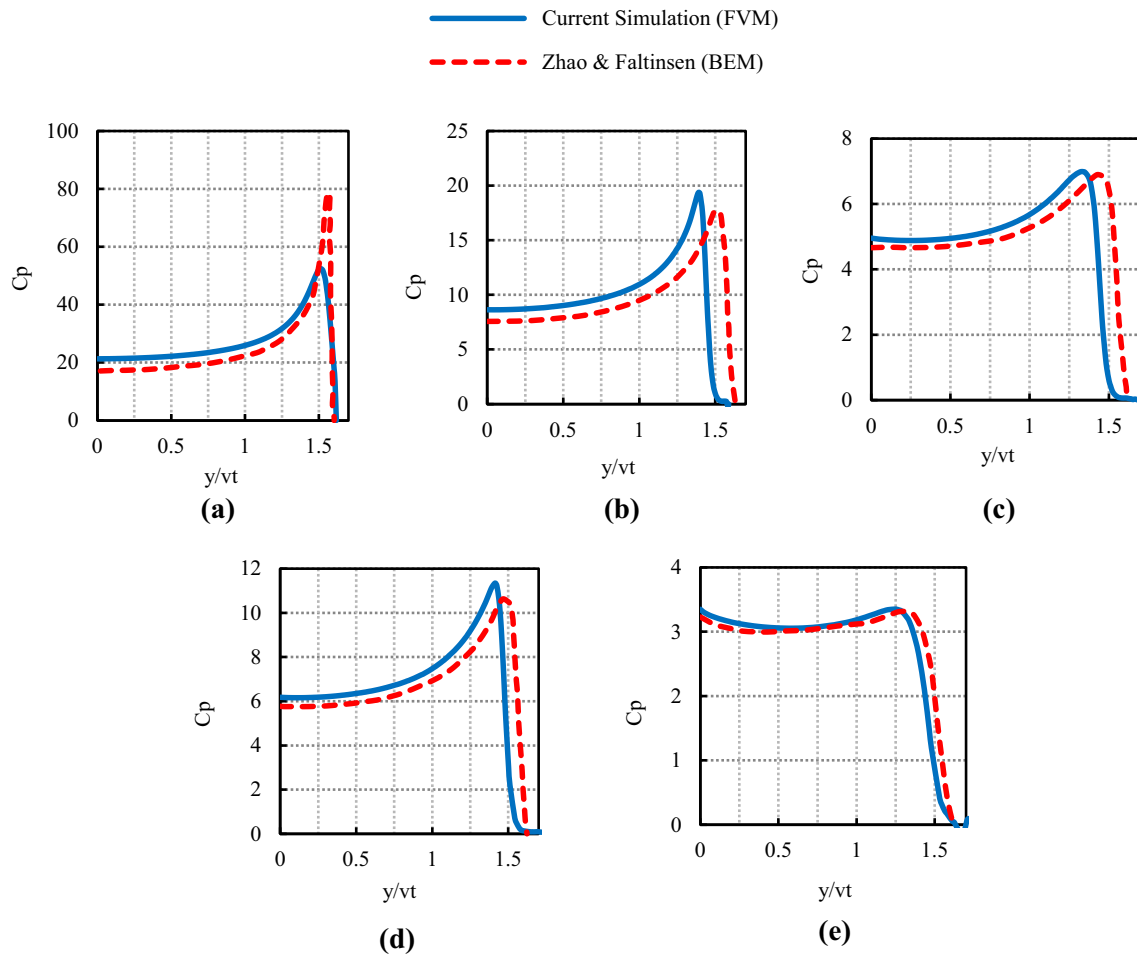


**Fig. 6** Comparison of the predicted pressure distribution over the wedge wall against numerical results of Zhao and Faltinsen [20] for water entry of wedge with constant speed: **a**  $\beta = 10^\circ$ , **b**  $\beta = 20^\circ$ , **c**  $\beta = 25^\circ$ , **d**  $\beta = 30^\circ$ , and **e**  $\beta = 45^\circ$

**Table 3** Run conditions

Run No.	Wedge width (m)	Deadrise angle ( $^\circ$ )	Drop height (m)	Mass (kg)
Run for W1				
1	0.61	10	0.61	124
Runs for W2				
2	0.61	20	0.61	124
3	0.61	20	1.22	124
4	0.61	20	1.83	124
5	0.61	20	0.61	293
6	0.61	20	1.22	293
7	0.61	20	1.83	293
Run for W3				
8	0.61	30	0.61	124

0.122 m are smaller than those of the lighter load. Even at the largest drop height, the accuracy of the heavier load is better than that of the lighter load. This can be attributed to the load force. When the load force is larger, the difference between the impact force and the load force decreases, and

leads to smaller acceleration. When this occurs, the vertical impact changes at a smaller rate which yields smaller variations in the fluid velocity field with respect to time. Hence, the current numerical method provides better accuracy in predicting the dynamic response of the heavier

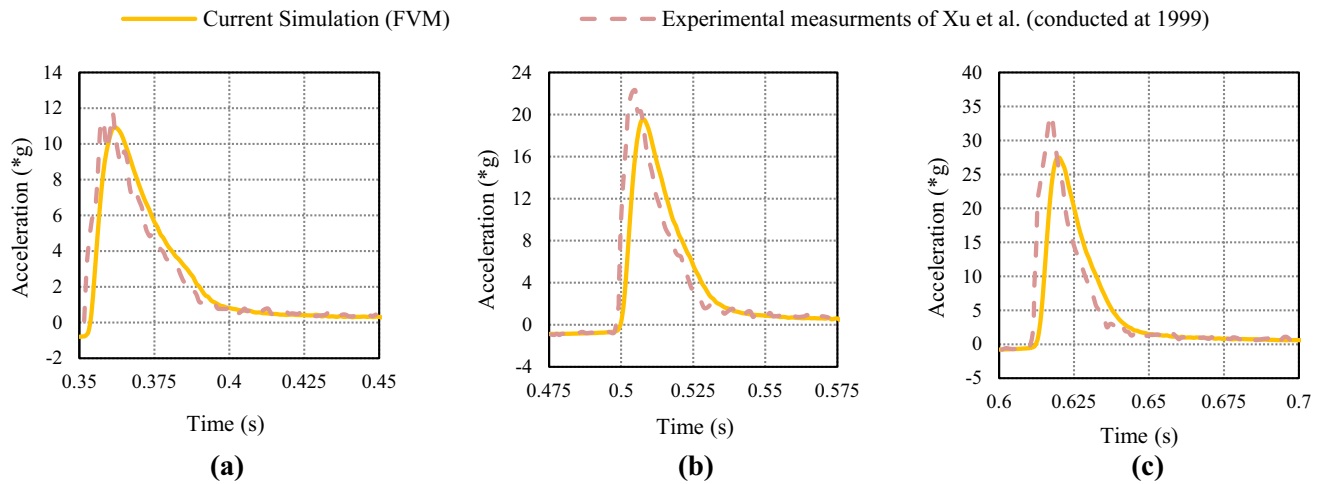


**Fig. 7** Comparison of the predicted vertical acceleration against experimental data of Xu et al. [22] for the W2 model with mass of 124 kg: **a**  $h_0 = 0.61$  m, **b**  $h_0 = 0.122$  m, and **c**  $h_0 = 0.183$  m

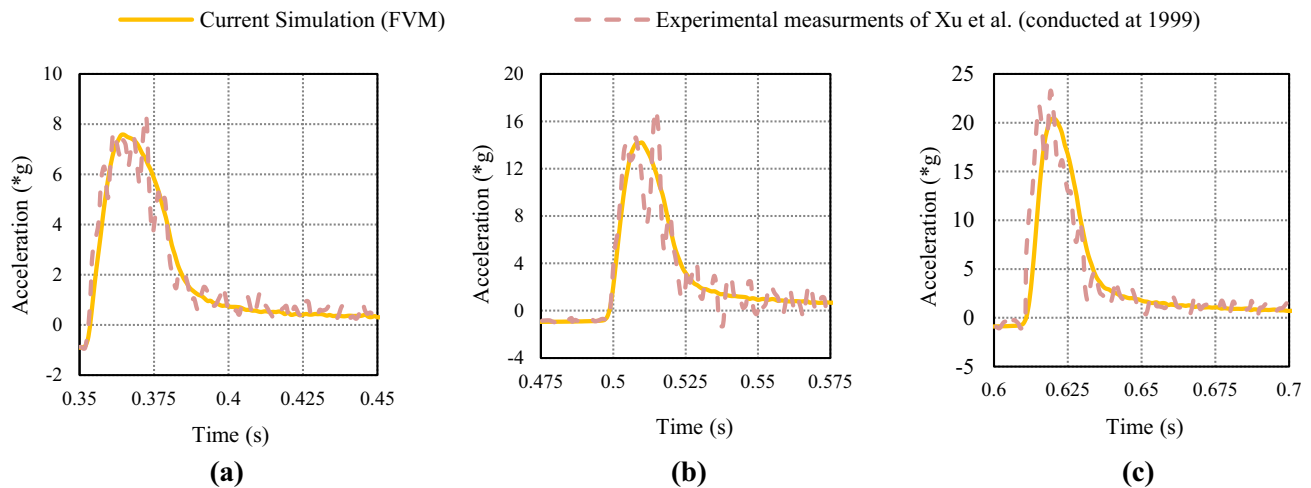


**Fig. 8** Comparison of the predicted vertical acceleration against experimental data of Xu et al. [22] for the W2 model with mass of 249 kg: **a**  $h_0 = 0.61$  m, **b**  $h_0 = 0.122$  m, and **c**  $h_0 = 0.183$  m

loads. Moreover, based on the produced plots in this case, some fluctuations are observed in reported results by Xu et al. [22], which are not observed in the results of the current simulations. The vibration of the wedge wall during the impact causes these fluctuations, and since the current work does not deal with hydro-elasticity, these fluctuations are not determined.

#### 4.4 Comparison with recent experimental results of Panciroli and Porfiri [46]

To provide a better understanding regarding the capability of the presented numerical simulation, a comparison of the current results against the recent experimental results of Panciroli and Porfiri [46] is also presented. Therefore, a wedge falling into water with deadrise angle of  $25^\circ$  and the

initial drop height of 50 and 75 cm are considered. The weight of the wedge is set to be 0.46 kg. The obtained results are displayed in Figs. 9 through 11. Figure 9 shows the predicted acceleration. As evident in this figure, the trend of variation of the predicted vertical acceleration, as a function of time, is similar to experimental results of Panciroli and Porfiri [46], showing that the current numerical simulation is relatively accurate. Figure 10 displays the predicted normal force per unit depth. According to this figure, the behavior of the predicted force, as a function of time, is also similar to the experimental data for both the initial heights. In addition to this, the peak values of both experimental data and the current numerical data are also in good agreement, especially for the case with the initial height of 75 cm. Ultimately, the predicted vertical speeds at different times are compared against the



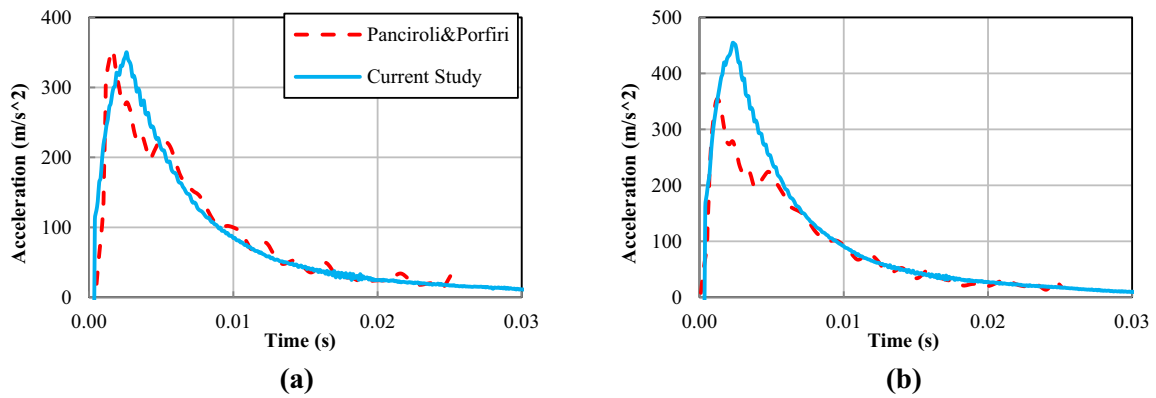


**Fig. 9** Comparison of the predicted vertical acceleration (dashed line) against experimental data of Panciroli and Porfiri [46] (solid line): **a** initial height of 50 cm and **b** initial height of 75 cm

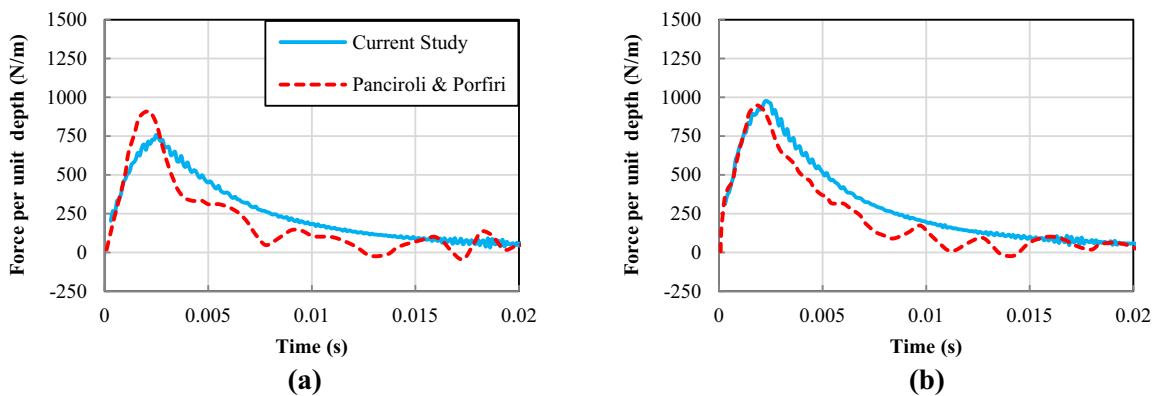


**Fig. 10** Comparison of the predicted normal force (dashed line) against experimental data of Panciroli and Porfiri [46] (solid line): **a** initial height of 50 cm and **b** initial height of 75 cm

theoretical solution of Wagner [8], as shown in Fig. 11. Plots of this figure suggest that the computed vertical velocity through the current numerical method displays good agreement with the theoretical solution of Wagner [8].

A comparison between normalized pressure of the current numerical simulation and experimental results of Panciroli and Porfiri [46] is displayed in Fig. 12. As evident in this figure, the results of current numerical simulation agree with experimental data and theoretical solutions of Wagner, especially near the peak pressure, and

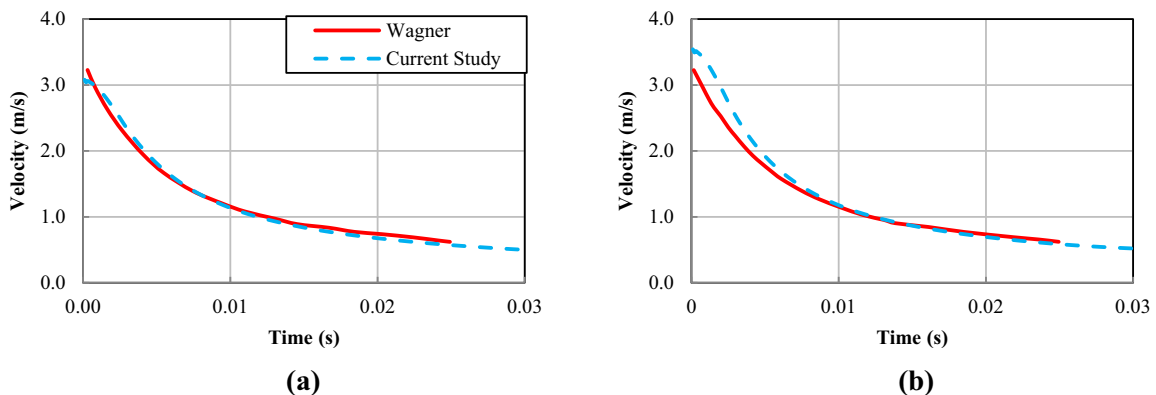


**Fig. 11** Comparison of the predicted vertical velocity (dashed line) against theoretical solution of Wagner [8] (solid line): **a** initial height of 50 cm and **b** initial height of 75 cm

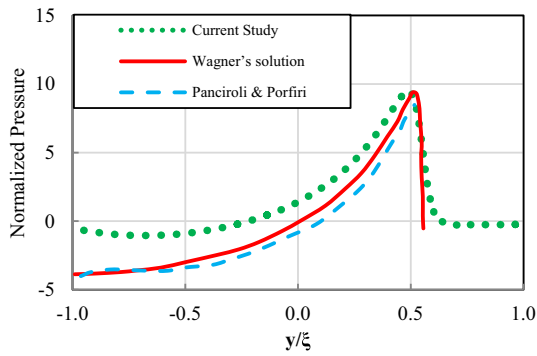


**Fig. 12** Comparison of the predicted normal normalize pressure acting on the wedge considered wedge with experimental results of Panciroli and Porfiri [46] and Wagner's solution [8]

the error in predicting the peak pressure is smaller than 10%.

The computed pressure contours in the fluid domain are compared against experimental data for both the initial heights, as shown in Figs. 13 and 14. This comparison shows that the computed pressure is very similar to the experimental data. For example, the normalized pressure counter near the water pile up of the initial height of 50 cm at  $t = 5$  ms is predicted to be 7.7, while experimental results of Panciroli and Porfiri [46] show that this value is about 7. On the other hand, the normalized pressure near

the wedge apex is predicted to be 1.7 at this initial height and time, while Panciroli and Porfiri [46] reported this value to be 2.0.

The results of the current simulations are compared against experimental data of Shams et al. [49] who modeled asymmetric freefall of a wedge of  $37^\circ$  deadrise angle. In a particular case of their experiments, they measured impact force acting on the wedge during symmetric impact. This wedge has a beam of 200 mm, and its mass is 0.631 kg, while the initial drop height is 50 cm. The predicted force per unit depth in this case is compared against experimental data, as shown in Fig. 15. Good compliance is observed in this comparison. The trend of experimental plot and numerical curve is similar. They both reach maximum value at  $t = 0.005$  s, and the rate of variation of force, as a function of time, is similar for both cases. The accuracy in predicting the force is also comparatively good.

Pressure distribution plots for a wedge of a  $37^\circ$  deadrise angle are also shown in Fig. 16. In this figure, experimental measurements of Shams et al. [49] as well as theoretical simulation of Wagner [8] are shown. It can be seen that the current numerical model predicts pressure with better accuracy than the theoretical method of Wagner [8] at all moments.

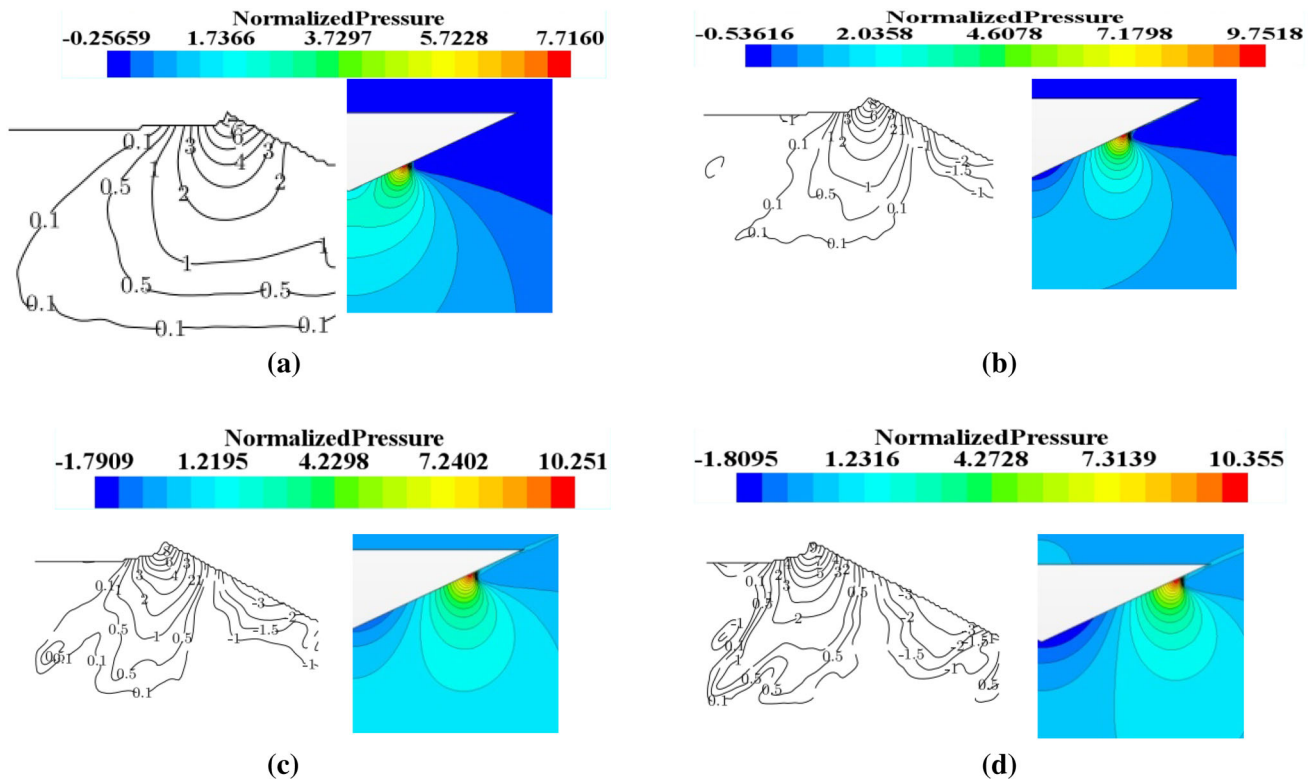


**Fig. 13** Comparison of the predicted pressure contours (colored contours) against experimental measurements of Panciroli and Porfiri [46] (solid line contours) for the wedge with deadrise angle of  $25^\circ$  at initial height of 50 mm at **a**  $t = 5$  ms, **b**  $t = 10$  ms, **c**  $t = 15$  ms, and **d**  $t = 20$  ms

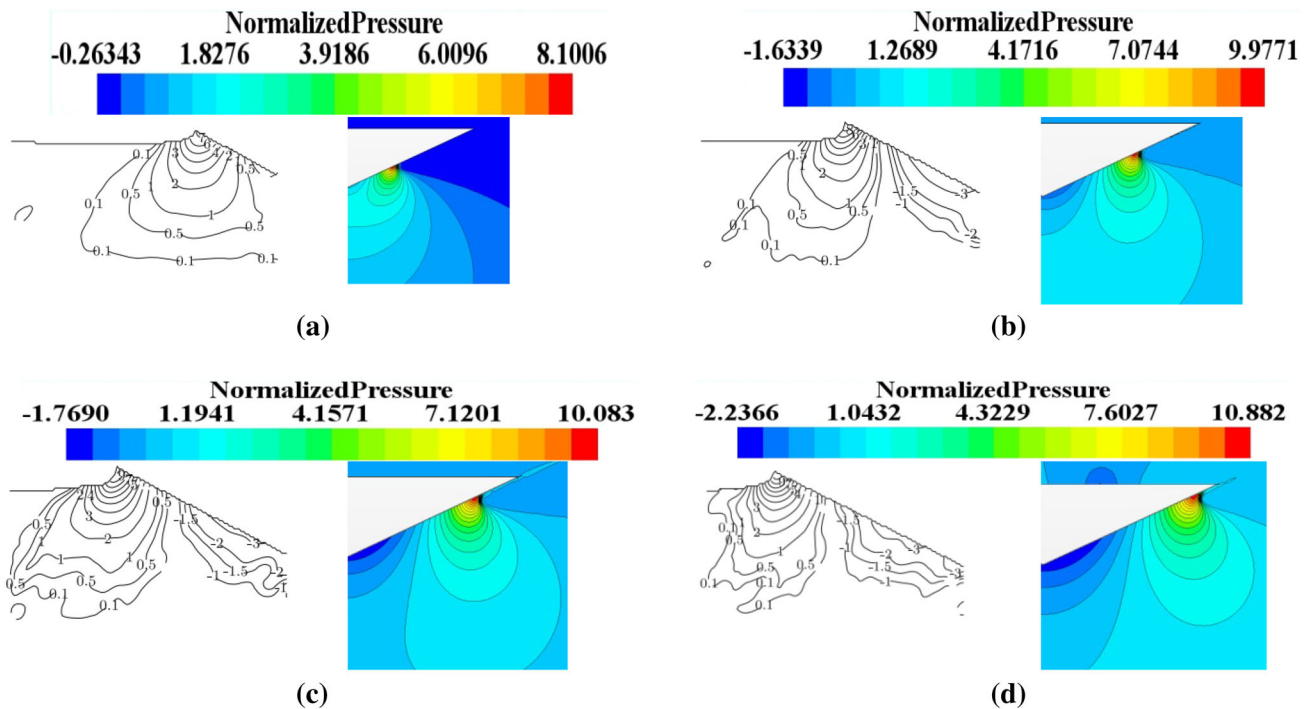


**Fig. 14** Comparison of predicted pressure contours (colored contours) against experimental measurements of Pancirol and Porfiri [46] (solid line contours) for the wedge with deadrise angle of 25° at initial height of 50 mm at **a**  $t = 5$  ms, **b**  $t = 10$  ms, **c**  $t = 15$  ms, and **d**  $t = 20$  ms

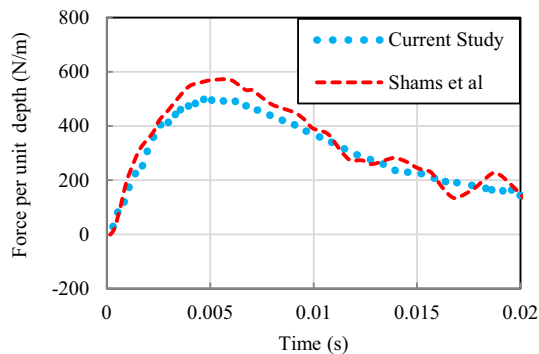


**Fig. 15** Comparison of the predicted normal force against experimental data of Shams et al. [49] for freefall of a wedge with deadrise angle of 37° at the initial height of 50 cm

## 5 Results

### 5.1 Kinematics of the wedges

The results of the conducted simulations identified in Table 2 are presented in this section. The predicted velocities for W2 model in both lighter and heavier load conditions are illustrated in Fig. 17. As evident in this figure, the plot of vertical velocity, as a function of time, displays three phases. The first phase is associated with the time at which the wedge has not reached the water, yet. During this time, speed linearly increases. The second stage is associated with a very short period of time, nearly

1–1.5 ms. During this time, the velocity abruptly decreases, mainly due to the occurrence of maximum vertical acceleration at this time. However, since the peak of acceleration lasts about 1–1.5 ms, this sudden change ends very quickly. This phase is called the onset of the impact, the time at which water impacts the wedge surface. The last phase starts right after the mentioned abrupt change. During this phase, the wedge velocity decreases at a slower rate and reaches zero or a constant value. A comparison between different considered cases can offer some more insights into these three phases. As expected, the larger drop height leads to larger value of vertical velocity at the end of the first phase. The slopes of speed versus time plots for all three cases are identical in this phase, since all of them are exposed to gravitational acceleration. During the second phase, the cases with the largest drop height experiences more abrupt decrease at their speed. However, its vertical speed is still larger than that of other cases. More sudden decrease is caused by the larger maximum acceleration. At the final phase, speed in all three cases decreases with nearly similar slope.

A comparison of the kinematics related to runs 1, 2, and 8 is displayed in Fig. 18. As evident in Table 3, all of these runs have the same drop height and same mass, while their deadrise angles are different (deadrise of W1, W2, and W3 models is, respectively, 10°, 20°, and 30°). Based on the results in this figure, it can be concluded that W1 model has the largest vertical speed, while W3 model has the

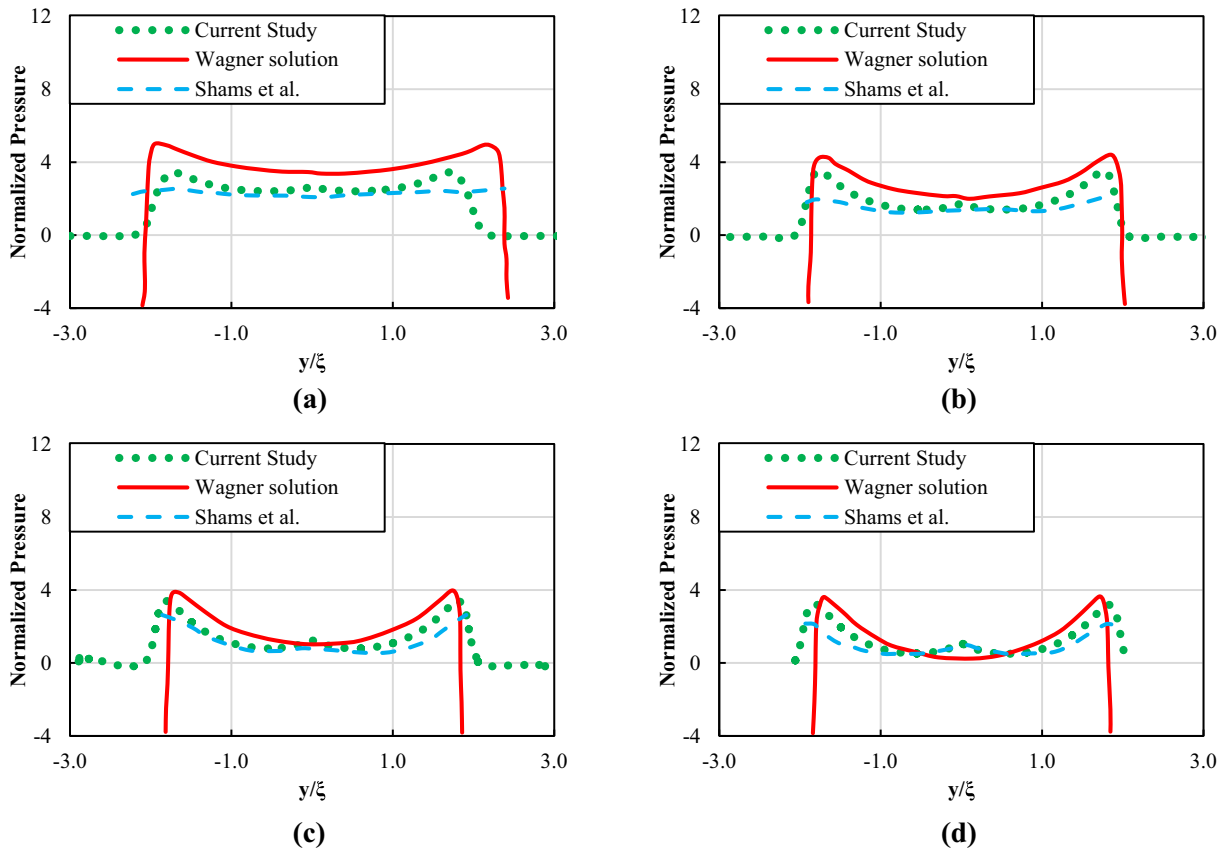
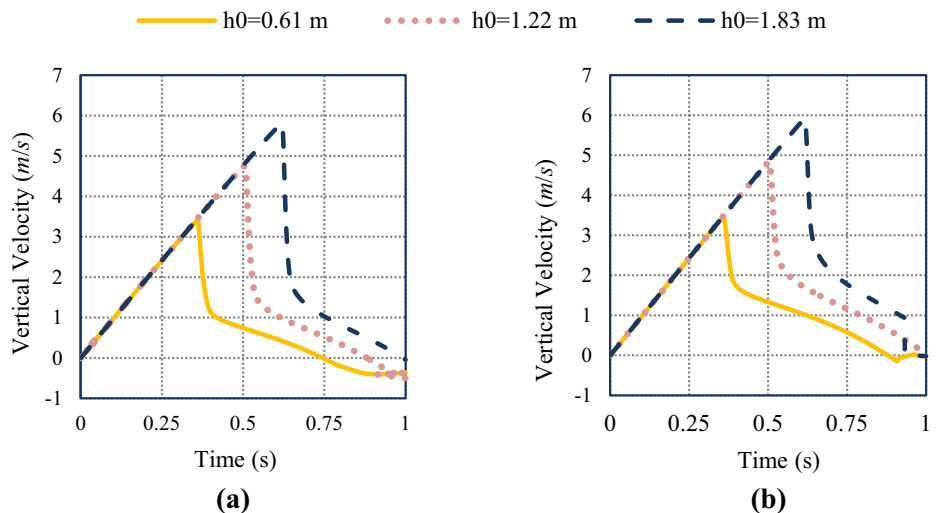


**Fig. 16** Comparison of the predicted pressure against experimental data of Shams et al. [49] for the freefall of a wedge with deadrise angle of  $37^\circ$  at initial height of 50 cm: **a**  $t = 5$  ms, **b**  $t = 10$  ms, **c**  $t = 15$  ms, and **d**  $t = 20$  ms

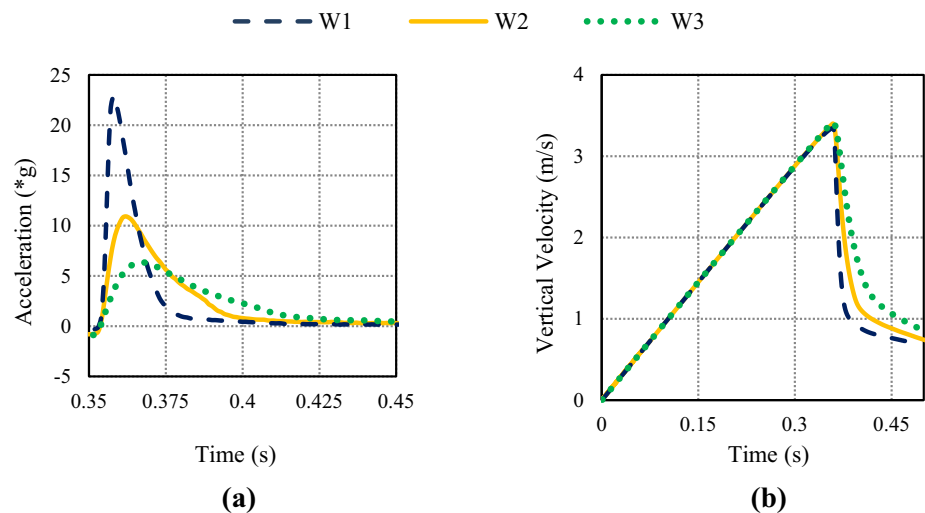
**Fig. 17** Predicted vertical velocity for W2: **a** mass of 249 kg and **b** mass of 249 kg



smallest vertical speed. This implies that a wedge of smaller deadrise angle reaches larger vertical acceleration at the onset of the impact. This occurs due to the fact that smaller deadrise angle is more similar to a plate, as water on its surface covers more area and spray root cannot move up as readily as the larger deadrise angles. All of these

factors together lead to larger vertical acceleration at the beginning of the penetration of W1 model. Furthermore, it can be seen that the time, during which the maximum vertical acceleration drops, is different for each of these cases. This time lasts the least for W1 model, and has the largest value for W3 model. It is noteworthy that, after all

**Fig. 18** Comparison of the results of the kinematics of W1, W2 and W3 models with drop height of 0.61 m and mass of 124 kg against each other: **a** vertical acceleration and **b** predicted vertical velocity



wedges transit from a vertical acceleration to a small acceleration, they all reach nearly similar values.

Based on the results of the vertical velocity, it can be seen that all three wedges reach similar value right before the beginning of the penetration, since they have the same weight and fall from an identical height. The obtained results suggest that vertical speed of W1 model, the wedge of  $10^\circ$  deadrise angle, drops with the largest rate. On the contrary, velocity of W3 model decreases with the slightest rate. This behavior of the vertical velocity occurs, due to the fact that the wedge with smaller deadrise angle has larger vertical acceleration. When the deadrise angle is larger, the spray root can move up more easily than the smaller deadrise angle. Therefore, it produces smaller force against the wedge penetration. This indeed proves that a wedge with smaller deadrise angle experiences smaller variations in its speed.

## 5.2 Impact loads of the wedges

The impact forces acting on W2 model during the freefall are shown in Fig. 19. In this figure, results of all six run conditions related to W2 model are displayed. Some interesting points can be inferred from the displayed results. The first point corresponds to the magnitude of the vertical force, which is intensified with an increase in the drop height. As observed in this figure, when the drop height doubles, the impact force becomes a little smaller than twice of its previous value. This can also be seen for the drop height of 1.83 m which is three times of 0.61, while its maximum vertical acceleration (74.3) is smaller than three times of the vertical acceleration (28.13), caused by the drop height of 0.61. On the other hand, it is observed that vertical force reaches a maximum value and then decreases, and subsequently reaches a very small value, a value slightly larger than zero. The time during which force

decreases is considered to be the instant when the force exerts its structural effects on the wedge. As shown in Fig. 19, when the drop height increases, this period reduces. This can be attributed to the larger force caused by the fluid. Since larger drop height leads to larger impact force, the wedge reaches a constant speed earlier, in comparison with the smaller drop height. As a result, the force acting on the wedge diminishes faster.

The computed impact force for three different wedges consisting of W1, W2 (run No. 2), and W3 models is displayed in Fig. 20. The wedge with the smallest deadrise angle, i.e., W1 model, has the largest impact force. The geometry of the wedge which is more similar to a flat plate than the other cases displays this behavior. In addition, the time during which impact force has large values is the longest for W3 model. This basically implies that the larger deadrise angle is exposed to significant impact force for a more extended time. A wedge with smaller deadrise angle blocks the water path in the upward direction, directing it toward the left and right sides of the wedge. This is while, on the surface of a wedge with larger deadrise angle, this does not happen, and instead, the water moves up easily. Therefore, the impact force is applied to the wedge for a longer period of time in the case of larger deadrise angle.

To provide a better understanding regarding the impact loads, time histories of the dynamic pressure are presented at three different points on the wedge wall. The first point is placed at the apex of the wedge (called keel probe), the second one is set at the middle of the wedge (called middle probe), and the third one is located between these two (called quarter probe). Time history of the pressure for W2 model in the lighter case is displayed in Fig. 21. Based on an overall view of the presented plots, one may conclude that the pressure at each probe is zero at first, and then, it suddenly reaches a maximum value. Ultimately, the pressure at the probe reduces and reaches a constant value. It

**Fig. 19** Impact force acting on W2 model during the freefall:  
**a**  $m = 124$  kg and  
**b**  $m = 249$  kg

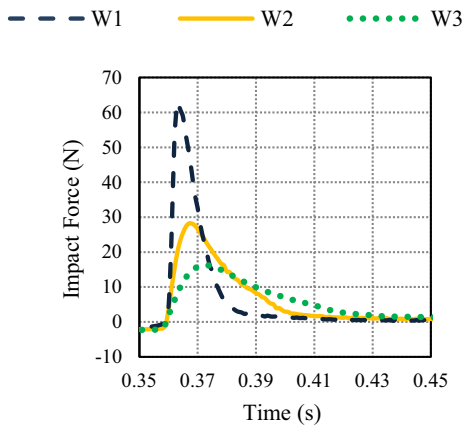
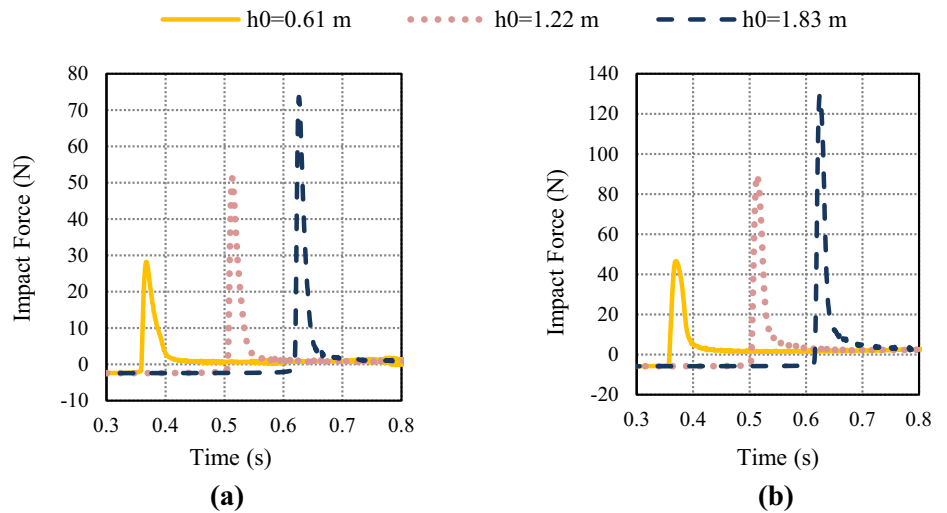


**Fig. 20** Comparison of the impact forces acting on W1, W2 (run No. 2), and W3 models

should be noted that maximum pressure at a probe occurs when the water reaches that probe. It is interesting that maximum pressure of the keel probe is larger than that of the quarter probe, and maximum pressure of the latter is larger than that of the middle probe. When water reaches the keel at the commencement of the impact, the wedge has its largest vertical velocity (see Figs. 17 and 18), and the wetted surface of the wedge is very small. However, as the water moves upward on the wedge wall, the velocity decreases and the wetted surface becomes larger. These two factors together cause the pressure to decrease as the wedge penetrates more into the water. This is why the quarter probe has smaller pressure than the keel probe and larger pressure than the middle probe. Finally, it should be mentioned that an increase in the drop height yields larger pressure, as shown in Fig. 21. When the wedge falls from a

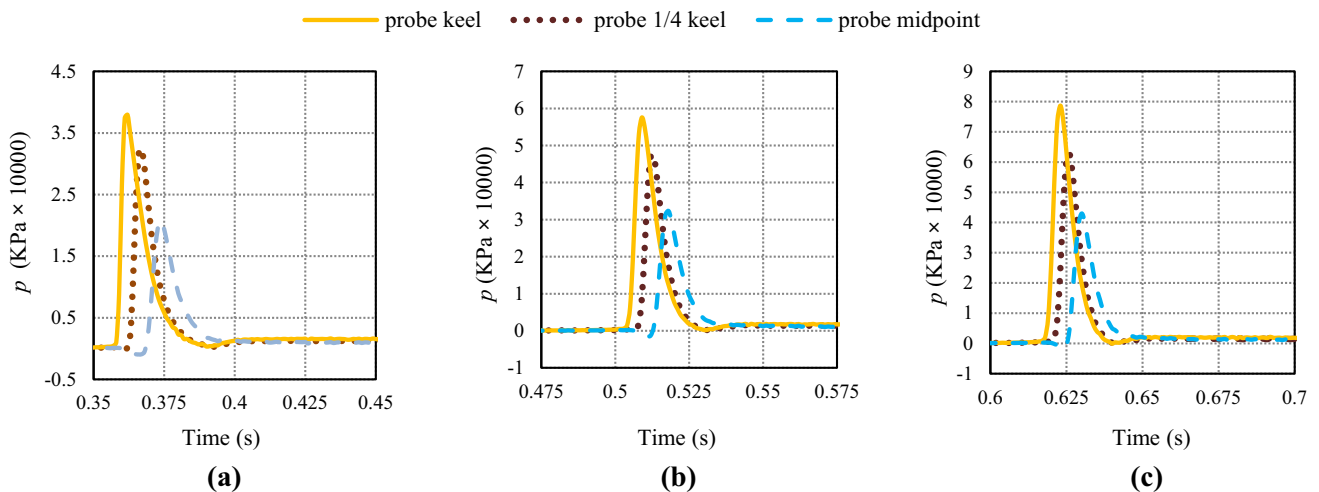


**Fig. 21** Time histories of the pressures at three different defined probes for W2 model with mass of 124 kg: **a**  $h_0 = 0.61$  m, **b**  $h_0 = 0.122$  m, and **c**  $h_0 = 0.183$  m

larger drop height, it impacts the water with larger speed, and as a result, the pressure acting on it increases. The computed time history of the pressure at this probe for the heavier case is demonstrated in Fig. 22. Similar to what was observed in the previous case, an increase in the drop height causes an increase in the pressure.

A comparison of the pressure time histories for W1, W2, and W3 models is displayed in Fig. 23. Pressure time tracks on the keel probe and the middle probe are determined. According to the graphs presented in this figure, it may be concluded that an increase in the deadrise angle leads to a larger pressure at both probes. The underlying reason behind this fact was explained earlier.

In addition to time history of the pressure, its distribution over the wedge wall is also presented. These results offer more insights into the effects of the freefall on the pressure distribution. Pressure distribution on the wetted surface of W2 model with mass of 124 kg is illustrated in Fig. 24. Here, the vertical axis represents the pressure coefficient normalized by  $p/(0.5\rho v^2)$ , while the horizontal axis represents the vertical distance from the wedge apex, non-dimensionalized as  $y/d$  ( $d$  is the wedge depth beneath the water surface at each instant). Pressures at four different times are presented for each case (Run 2 through 7). Results in Fig. 24 imply that as time passes and the vertical acceleration decreases, the peak pressure decreases, while the area of maximum pressure shifts outward. Based on what was described earlier about the acceleration, its value abruptly decreases and when this happens, the pressure in vicinity of the spray root is expected to increase. It is notable that Facci et al. [50] observed similar behavior for a solid wedge in freefall motion.

It can, furthermore, be seen that the difference between pressures at the first recorded instant and the last recorded

instant becomes larger when the drop height increases. As pointed out earlier, the cases with larger drop height experience a faster decrease in pressure. Therefore, as time passes, acceleration drops more, yielding further decrease in the pressure.

The computed pressure for W2 model with mass of 249 kg is displayed in Fig. 25. Similar to what was seen in the lighter case, a decrease in the pressure coefficient occurs when the entry depth increases. Based on a comparison of the results in this case with those in the lighter case, it can be concluded that pressure is slightly larger in the heavier cases.

### 5.3 Free surface

In addition to the impact loads and kinematics of the wedge, the wetted surface is also important to be investigated, simply because it can provide good information regarding that part of the structure, which is exposed to the impact load. Free surface elevation around W2 model during the freefall from the height of 0.61 m is presented in Fig. 26 for two different masses. The horizontal axis is non-dimensionalized using  $c$ , the half beam soaked by calm water, and the vertical axis is normalized using  $d$ , the submerged height of the wedge. Based on the comparison of the results in different instances, it can be concluded that as the wedge enters the water further, the water pile-up increases. The acceleration decrease in time is the underlying factor behind this phenomenon. At the initial times of the impact, the acceleration is large, and as a result, the water does not have sufficient time to slip over the wedge wall. However, as time passes and acceleration decreases, the water has enough time to slide over the wedge.

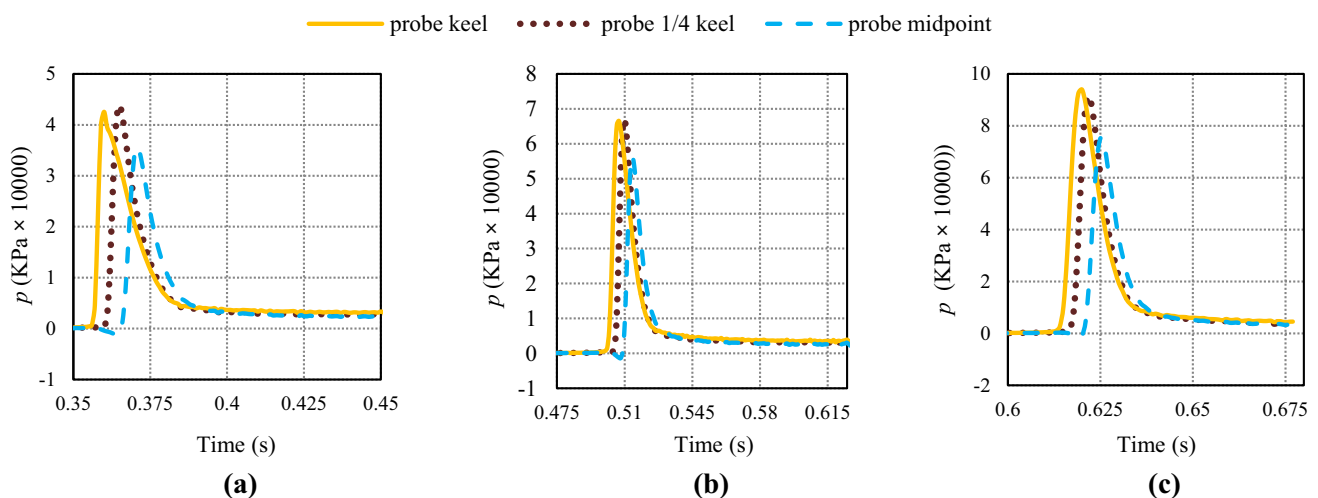


**Fig. 22** Time histories of the pressures at three different defined probes for W2 model with mass of 249 kg: **a**  $h_0 = 0.61$  m, **b**  $h_0 = 0.122$  m, and **c**  $h_0 = 0.183$  m

**Fig. 23** Comparison of time history of pressure at two different defined probes for W1, W2 (run No. 2), and W3: **a** keel probe and **b** middle probe

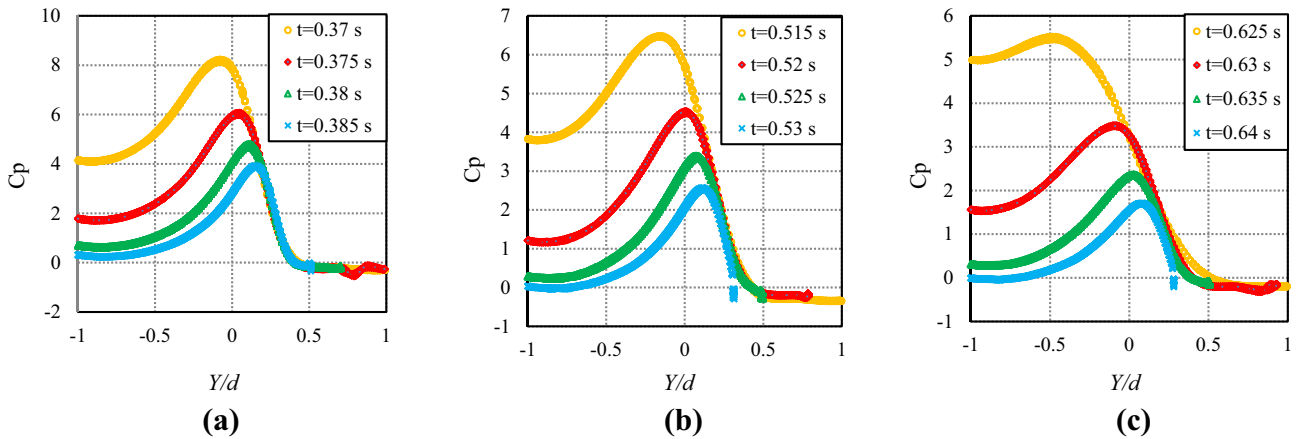
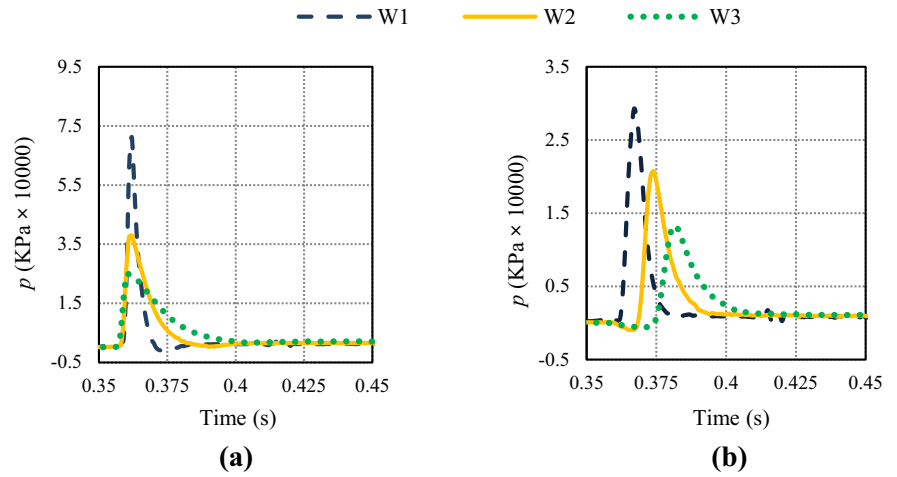


**Fig. 24** Computed pressure over the wall of W2 model with mass of 124 kg during freefall: **a**  $h_0 = 0.61$  m, **b**  $h_0 = 0.122$  m, and **c**  $h_0 = 0.183$  m

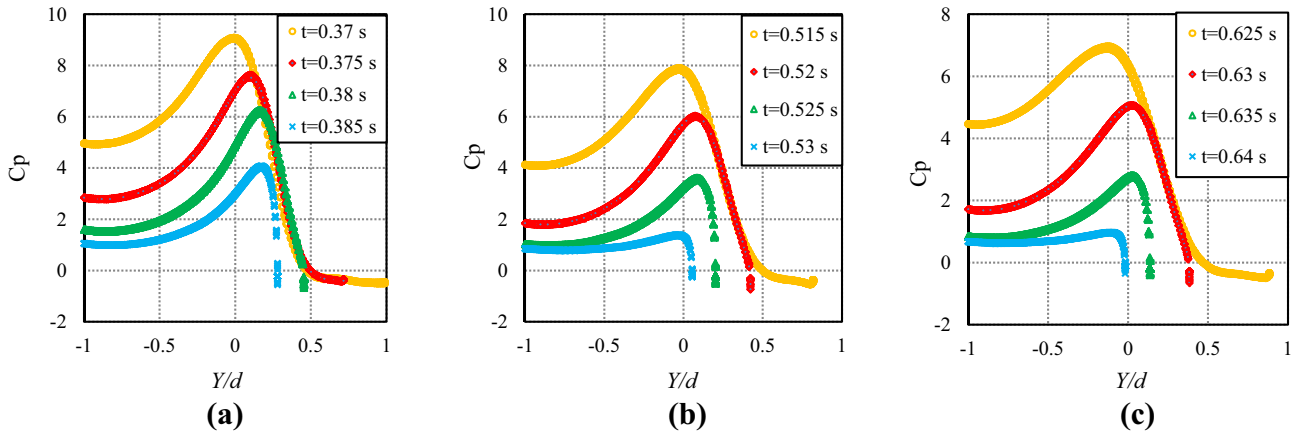


**Fig. 25** Computed pressure over the wall of W2 model with mass of 249 kg during freefall: **a**  $h_0 = 0.61$  m, **b**  $h_0 = 0.122$  m, and **c**  $h_0 = 0.183$  m

The free surface elevations for W1 and W3 models are also displayed in Fig. 27. The presented results indicate that there is a minor difference between the free-surface

profiles of W3 model in different conditions. This implies that when the deadrise angle increases, the variation of the free surface profile with time becomes less significant. As



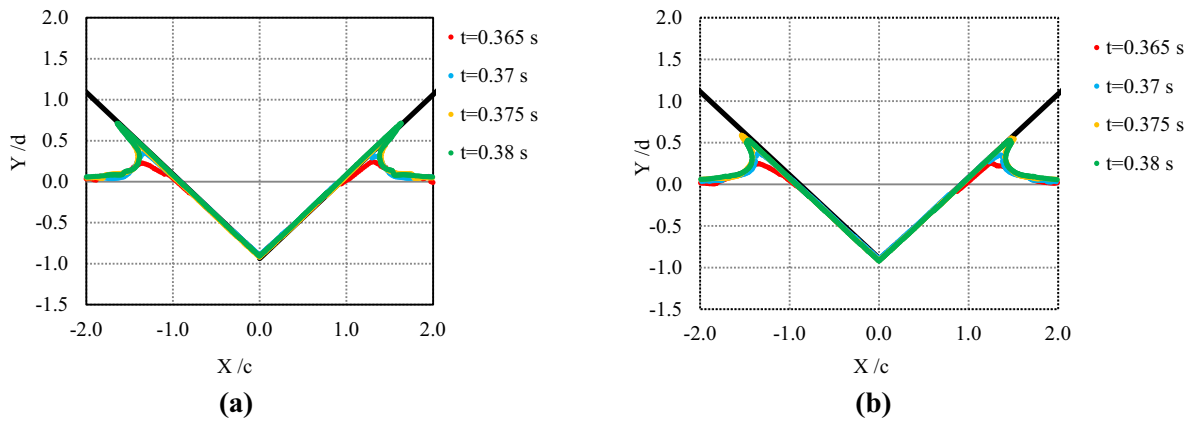


**Fig. 26** Free surface elevation around W2 model during freefall from the height of  $h_0 = 0.61$  m: **a** mass of 124 kg and **b** mass of 249 kg

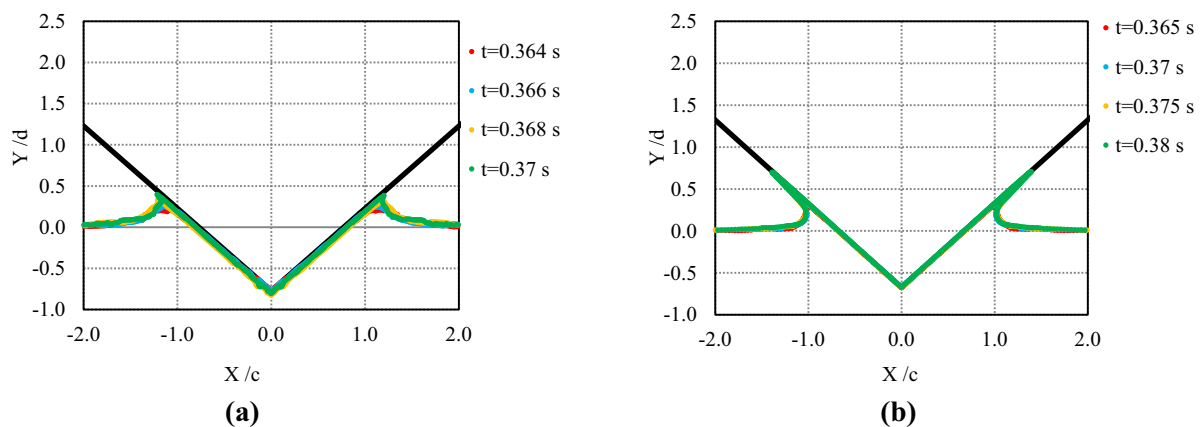


**Fig. 27** Free surface elevation around **a** W1 and **b** W3 models

observed and stated earlier, the wedge with larger deadrise angle experiences smaller acceleration during the early stage of the penetration, thereby the water pile-up is not affected lesser in comparison with that of smaller deadrise angle case.

Finally, it should be noted that the proposed numerical model has utilized an FVM-based code for solving the defined problem. This code provides an opportunity to consider the effect of viscosity in the targeted simulations which cannot be taken into account by the BEM method. On the other hand, this method can easily provide the velocity and pressure contours in the fluid domain, but through BEM approach, the boundary conditions are considered to be linear, which can reduce the accuracy of the solution in predicting the water surface elevation. Although BEM method can provide a faster simulation of the problem and may be used for different ship sections through strip theory, free-surface elevation can be captured much easier with better accuracy using coupled FVM-VOF scheme. Furthermore, by adopting this approach, the thin spray breaking into water drops can also be better modeled.

## 6 Conclusions

In the current paper, freefall of different wedges into the water surface is investigated. To analyze the targeted simulations, the STAR CCM+ software is utilized which applies the FEM based FVM for solving the momentum and mass continuity equations. Free surface of the water is modeled using volume fraction approach and HRIC scheme. Three different wedges of  $10^\circ$ ,  $20^\circ$ , and  $30^\circ$  deadrise angles, respectively, named W1, W2, and W3 models, are studied. Among the three considered wedges, the W2 model has previously been experimentally studied and is hereby used for validation purposes.

Main results of the current research include kinematics, loads, and free surface elevation around the wedge. Accordingly, vertical acceleration of W2 model is computed and compared against experimental data and good agreement is achieved. It is further observed that vertical acceleration of the larger deadrise angle is larger and diminishes faster. The result of the vertical speed is also displayed and it is concluded that in similar initial condition, the speed of larger deadrise angle drops, more rapidly.

After studying the kinematics of the considered wedges, impact loads and pressure are explored. The computed impact loads indicate that W1 model, which has the smallest deadrise angle, has the largest impact force, while W3 model, which has the largest deadrise angle, has the smallest impact force. Moreover, it is expectedly observed that an increase in the initial drop height yields a larger force. Time histories of the pressure are determined at three different probes for W2 model. The results indicate that pressure reaches a maximum value, as the point is drenched, and then immediately drops. As the distance from the keel increases, this maximum value is reduced. The maximum pressure is observed to be larger when the deadrise angle reduces. Furthermore, larger drop height causes a larger pressure peak. Afterward, the pressure distribution over the wedge wall is presented, indicating that as the wedge penetrates the water more and more, the pressure coefficient decreases. It is also observed that this decrease becomes more significant when the dropped height increases.

Ultimately, the free-surface elevation near the wedge is computed. Based on the obtained results, as the submergence height of the wedge increases during the freefall, the pile-up increases. This increase becomes less effective when the deadrise angle increases.

The provided kinematics, impact loads, pressure coefficients, and free-surface elevation for the wedges of  $10^\circ$ ,  $20^\circ$ , and  $30^\circ$  deadrise angles in the current paper can empower the engineers for efficient design of the structure of high-speed crafts in more realistic conditions. In future studies, it is necessary to consider more degrees of freedom for the wedge that can offer better understanding of the freefall of wedges, and can provide new information regarding the impact loads and kinematics of the wedges when they fall into the water without any restriction in angular and horizontal directions.

## References

- Faltinsen OM, Landrini M, Greco M (2007) Slamming in marine applications. *J Eng Math* 74(3–4):187–217
- Ghadimi P, Tavakoli S, Dashtimanesh A, Zamanian R (2016) Steady performance prediction of heeled planing boat in calm water using asymmetric 2D + T model. *Proc Inst Mech Eng Part M*. <https://doi.org/10.1177/1475090216638680>
- Akers RH (1999) Dynamic analysis of planing hulls in the vertical plane. In: Meeting of the New England Section of the Society of Naval Architectures and Marine Engineers
- Ghadimi P, Tavakoli S, Dashtimanesh A (2016) Coupled Heave and pitch motions of planing hulls at non-zero heel angles. *Appl Ocean Res* 59:286–303
- Ghadimi P, Tavakoli S, Dashtimanesh A (2016) An analytical procedure for time domain simulation of roll motion of the warped planing hulls. *Inst Mech Eng Part M* 230(4):600–615
- Morabito MG (2015) Prediction of planing hull side forces in yaw using slender body impact theory. *Ocean Eng* 101:47–57
- von Karman T (1929) The impact of seaplanes floats during landing. NACA TN 321
- Wagner H (1932) Phenomena associated with impacts and sliding on liquid surfaces. NACA Translation
- Howison SD, Ockendon JR, Wilson SK (1991) Incompressible water entry problems at small deadrise angles. *J Fluid Mech* 222:215–230
- Korobkin AA (1996) Water impact problems in ship hydrodynamics. In: *Advances in Marine Hydrodynamics*, Boston, USA
- Oliver JM (2002) Water entry and related problems, PhD Thesis, University of Oxford, UK
- Scolan YM, Korobkin AA (2001) Three-dimensional theory of water impact. Part 1. Inverse Wagner problem. *J Fluid Mech* 440:293–326
- Faltinsen OM, Chazhain M (2005) A generalized wagner method for three-dimensional slamming. *J Ship Res* 49(4):279–287
- Korobkin AA, Melenica S (2005) Modified Logvinovich model for hydrodynamic loads on asymmetric contours entering water. In: *Proceedings of the 20th Intern. Workshop on Water Waves and Floating Bodies*, Longyearbyen
- Qin L, Zhao J, Sing A (2011) A modified Logvinovich model For hydrodynamic loads on an asymmetric wedge entering water with a roll Motion. *J Mar Sci App* 10:184–189
- Mei X, Liu Y, Yue DKP (1999) On the water impact of general two-dimensional sections. *Appl Ocean Res* 21:1–15
- Yettou EM, Derochers A, Champoux Y (2007) A new analytical model for pressure estimation of symmetrical water impact of a rigid wedge at variable velocities. *J Fluids Struct* 23:501–522
- Ghadimi P, Saadatkah A, Dashtimanesh A (2011) Analytical solution of wedge water entry by using schwartz–christoffel conformal mapping. *Int J Model Simul Sci Comput* 2(3):337–354
- Semenov YA, Iafrati A (2006) On the nonlinear water entry problem of asymmetric wedges. *J Fluid Mech* 547:231–256
- Zhao R, Faltinsen OM (1993) Water entry of two-dimensional bodies. *J Fluid Mech* 246:593–612
- Vorus WS (1996) A flat cylinder theory for vessel impact and steady planing resistance. *J Ship Res* 40(2):89–106
- Xu L, Troesch AW, Vorous WS (2003) Asymmetric vessel impact and planing hydrodynamics. *J Offshore Mech Arctic Eng Trans ASME* 121(2):83–89
- Judge C, Troesch AW, Prelin M (2003) Initial water impact of a wedge at vertical and oblique angles. *J Eng Math* 48:279–303
- Stenius I, Rosn A, Juttenkeuler J (2007) Explicit FE-modeling of fluid-structure interaction in hull-water impacts. *Int J Shipbuild Prog* 53:1031–1121
- Stenius I, Rosn A, Juttenkeuler J (2008) Explicit FE-modeling of fluid-structure interaction in panel-water impacts. *Int J Shipbuild Prog* 54:111–127
- Wang S, Soares CG (2012) Analysis of water impact of symmetric wedges with a multi-material Eulerian formulation. *Int J Marit Eng* 154:191–206
- Wang S, Soares CG (2013) Slam Induced loads on bow-flared sections with various roll angles. *Ocean Eng* 67:45–57
- Wang S, Soares CG (2014) Numerical study on the water impact of 3D bodies by an explicit finite element method. *Ocean Eng* 78:73–88
- Wang S, Soares CG (2016) Experimental and numerical study of the slamming load on the bow of a chemical tanker in irregular waves. *Ocean Eng* 111:369–383
- Farsi M, Ghadimi P (2014) Finding the best combination of numerical schemes for 2D SPH simulation of wedge water entry for a wide range of deadrise angles. *Int J Naval Archit Ocean Eng* 6:638–651

31. Farsi M, Ghadimi P (2014) Effect of flat deck on catamaran water entry through smoothed particle hydrodynamics. *Inst Mech Eng Part M*
32. Farsi M, Ghadimi P (2015) Simulation of 2D symmetry and asymmetry wedge water entry by smoothed particle hydrodynamics method. *J Braz Soc Mech Sci Eng* 37(3):821–835
33. Chekab MAF, Ghadimi P, Farsi M (2016) Investigation of three-dimensionality effects of aspect ratio on water impact of 3D objects using smoothed particle hydrodynamics method. *J Braz Soc Mech Sci Eng* 38:1987–1998
34. Brizzolara S, Couty N, Hemundstad O, Lotan A et al (2008) Comparison of experimental and numerical loads on an impacting bow section. *Ships Offshore Struct* 3:305–324
35. Fairlie-Clarck AC, Tveitness T (2008) Momentum and gravity effects during the constant velocity water entry of wedge-shaped sections. *Ocean Eng* 35(7):706–716
36. Maki KJ, Lee D, Troesch AW, Vlahopoulos N (2011) Hydroelastic impact of a wedge-shaped body. *Ocean Eng* 38(4):621–629
37. Ghadimi P, Dashtimanesh A, Djeddi SR (2012) Study of water entry of circular cylinder by using analytical and numerical solutions. *J Braz Soc Mech Sci Eng* 37(3):821–835
38. Ghadimi P, Feizi Chekab MA, Dashtimanesh A (2014) Numerical simulation of water entry of different arbitrary bow sections. *J Naval Archit Marine Eng* 11(2):117–129
39. Ghadimi P, Feizi Chekab MA, Dashtimanesh A (2013) A numerical investigation of the water impact of an arbitrary bow section. *ISH J Hydraul Eng* 19(3):186–195
40. Shademani R, Ghadimi P (2016) Estimation of water entry forces, spray parameters and secondary impact of fixed width wedges at extreme angles using finite element based finite volume and volume of fluid methods. *Brodogradnja* 67:101–124
41. Shademani R, Ghadimi P (2016) Parametric investigation of the effects of deadrise angle and demi-hull separation on impact forces and spray characteristics of catamaran water entry. *J Braz Soc Mech Eng Sci*
42. Shademani R, Ghadimi P (2017) Asymmetric water entry of twin wedges with different deadrisers, heel angles, and wedge separations using finite element based finite volume method and VOF. *J Appl Fluid Mech* 10:353–368
43. Faltinsen OM, Kjaerland A, Nottevit A (1997) Water impact loads and dynamic response of horizontal circular cylinders in offshore structures. In: 9th Annual Offshore Technology Conference, Hudson, USA
44. Xu GD, Duan WY, Wu GX (2008) Numerical simulation of oblique water entry of an asymmetrical wedge. *Ocean Eng* 35:1597–1603
45. Xu GD, Duan WY, Wu GX (2010) Simulation of water entry of a wedge through free fall in three degrees of freedom. *Proc R Soc A* 466:2219–2239
46. Panciroli R, Porfiri M (2013) Evaluation of the pressure field on a rigid body entering a quiescent fluid through particle image velocimetry. *Exp Fluids* 54:1630–1642
47. Jalalisendi M, Osma SJ, Porfiri M (2015) Three-dimensional water entry of a solid body: a particle image velocimetry study. *J Fluids Struct* 59:85–102
48. Jalalisendi M, Shams A, Panciroli R, Porfiri M (2015) Experimental reconstruction of three-dimensional hydrodynamic loading in water entry problems through particle image velocimetry. *Exp Fluids* 56:1–17
49. Shams A, Jalalisendi M, Porfiri M (2015) Experiments on the water entry of asymmetric wedges using particle image velocimetry. *Phys Fluids* 27(2):027103
50. Facci AL, Panciroli R, Ubertini S, Porfiri M (2015) Assessment of PIV-based analysis of water entry problems through synthetic numerical datasets. *J Fluids Struct* 55:484–500
51. Facci AL, Porfiri M, Ubertini S (2016) Three-dimensional water entry of a solid body: a computational study. *J Fluids Struct* 66:36–53